The Particle Tracking Code BBCNI for Negative Ion Beams and its Application to BATMAN Upgrade

A. Hurlbatt[1, a)], F. Bonomo[1], N. den Harder[1], D. Wünderlich[1], U. Fantz[1], and the NNBI Team[1]

[1] *Max-Planck-Institut für Plasmaphysik, Boltzmannstr. 2, 85748 Garching, Germany*

[a)]Corresponding author: andrew.hurlbatt@ipp.mpg.de

Abstract. For the continued improvement and development of large negative hydrogen ion sources for NBI applications, beam characterisation is of critical importance for understanding and predicting the interaction of a large beam with, for example, a gas neutraliser system. As large ion beams are comprised of collections of individual beamlets, the relationship between the results of beam diagnostics and the physical properties of the beam is not a trivial one. Measured quantities come from the mixing of information from different beamlets, and the extraction of beamlet level data may not be possible. To establish the links between diagnostic results and beamlet behaviour, the particle tracking code BBCNI has been designed to forward calculate simulated diagnostics from particle level data, including beam emission spectroscopy (BES) and calorimeter measurements. Full traceability of these synthetic diagnostics allows features to be linked to specific particle populations and areas of the beam, providing a much-needed understanding of experimental results. In order to demonstrate the capability of the code, the first experimental BES results from the BATMAN Upgrade test facility are also presented. Measurements of beam divergence as calculated from real and synthetic data are shown to be in good agreement, and it is demonstrated how the code can give details of individual beamlet properties and how these build into synthetic diagnostic data.

INTRODUCTION

The next generation tokamak ITER is foreseen to have 33 MW of neutral beam injection (NBI) power across 2 beams [1] for heating and current drive purposes. These systems for ITER are required to have not just high power, but also a high energy of 1 MeV. This high energy means that NBI based on negative ions will be necessary. The operation of a source with all the required parameters has not yet been demonstrated, and research is ongoing at a number of facilities to ensure that the targets for the ITER beamlines are reached within the required schedule. Strong progress has recently been made by the ELISE test facility at IPP Garching [2], a half-size prototype of the ITER source, which continues to approach the ion currents specified by the ITER requirements. The SPIDER facility at the European Neutral Beam Test Facility (NBTF) has recently started operation [3], to investigate the operation of an ion beam the same size as the ITER design, and the full scale and full energy prototype MITICA [3] is under construction, also at the European NBTF. Although the progress towards the required ion beam currents is promising, work is still required on improving aspects of the beam quality. Specifically, the homogeneity and divergence of the resulting ion beam also have strict requirements, and these are difficult to achieve simultaneously with a high ion current [4].

Each of these ion sources consists of an RF generated plasma, a plasma expansion region, and a system of extraction and acceleration grids containing many individual apertures. A magnetic filter field, with a strength of a few mT, is used in the plasma expansion region to cool the plasma and reduce the number of co-extracted electrons. This field can cause inhomogeneities in the plasma density due to E×B drifts [5]. In addition, these negative ion sources use caesium to enhance the surface production of H^- ions on the front of the plasma grid (PG), the first grid in the acceleration system. This caesium can be distributed nonuniformly due to plasma inhomogeneities [6], leading to a nonuniform surface production rate. These nonuniformities both mean that a different negative ion current may

be extracted from each aperture, which in turn can lead to a different divergence of each beamlet [7].

As a result, large ion beams that are comprised of many individual beamlets may not be well characterised by global values, but instead could have a spread of current and power densities, as well as divergence. Due to the high power densities involved, the options for diagnosing such a beam are limited to those that measure some ensemble of beamlet. Direct measurement within the extraction system is not possible due to space constraints, but instead can only be performed downstream of the last grid, sometimes a number of metres away. Therefore the data obtained from beam diagnostics will inevitably be the result of a mixing of information from many different beamlets. For example, beam emission spectroscopy (BES) is used to measure the width of a Doppler shifted emission peak that is generated by the beam interacting with the background gas. This can then be used to calculate a value of divergence for the beam [8]. If each beamlet has its own properties, then it will also have its own emission spectrum. The spectra recorded by the BES diagnostic will be some non-trivial combination of these, and it is therefore not possible to know if the measured divergence truly reflects the divergence of the beam, or is instead affected in some way by the mixing of individual beamlet spectra.

The generation and transport of a large ion beam needs to be understood from the ion optics of individual beamlets, if sufficient improvements to the beam quality are to be made. Therefore the mixing of beamlet properties into diagnostic results needs to be unravelled, which cannot be done with the experimental data alone. This paper presents the use of the particle tracking code BBCNI for the forward calculation of simulated diagnostic results from particle level information. The traceability of the code is shown to allow the exploration of individual beamlet properties, and how these combine into synthetic diagnostic data. The application of experimental data analysis routines on the synthetic data is used to give a direct comparison point between the code and results from the BATMAN Upgrade Test Facility [9,10].

SIMULATING BEAM DIAGNOSTICS

As the purpose of simulating the beam diagnostics is to assist in untangling the superposition of many beamlets from their individual properties, the formation of each beamlet must be accurately modelled, as well as their position in 3D space with respect to the beam diagnostics and each other. Accurate simulation of the beamlets requires sub-millimetre resolution of particle positions and velocities in 3D due to the complex electric and magnetic field geometry caused by perpendicular magnetic fields [11]. These magnetic fields may not be uniform across the extraction area [12], and so each aperture could experience a unique magnetic field, leading to different beamlet formation and subsequently a different electric field. In addition, for beam focussing purposes, each beamlet may have a slightly different electrode configuration [13], or beamlets may be arranged so that they converge to a single point [14]. Thus the simulation needs to consider the creation of each beamlet individually as well as its transport from the extraction system to the beam diagnostics. This means encompassing length scales from the sub-millimetre upward in a domain metres in size, and energy scales from 1 eV to 1 MeV, in full 3D with electric and magnetic fields present. As this is impractical for a self-consistent PIC simulation, a reasonable compromise is particle tracking in pre-computed fields.

The Bavarian Beam Code for Negative Ions (BBCNI) has been designed specifically to fulfil these requirements for the simulation of large ion beams and their diagnostics. It was originally developed a number of years ago [15], but has recently undergone significant upgrades and enhancements. It comprises of a number of independent modules, and the code flow diagram in Fig. 1 shows the most important of these. In order to capture as many effects of ion optics as possible, the code simulates H^- ions starting on the plasma side of the PG. These ions are accelerated through the grid system by a pre-defined 3D electric field map present there. They continue to be tracked until they strike either the calorimeter or another surface. Magnetic fields are considered for the whole domain, and so their effect not just on the accelerating beamlets, but also on the final beam, is considered. Ions may undergo a reaction with the background gas at any time, forming fast and slow H atoms, fast H^+ ions, or slow H_2^+ ions, as well as the associated detached electrons. The final locations and properties of all particles are recorded, as are the specifics of any reaction that takes place. H^- ions and H atoms can both produce H_α photons weighted according to the expected reaction rate, which is found from the energy-specific cross sections [16,17] and the gas density at the current location. The records generated during the simulation, of particle destinations and generated photons, are post-processed into various statistical analyses to show beam properties either as they would be measured by real diagnostics, or in some way that cannot be measured in reality. A selection of possible outputs are shown on the right hand side of Fig. 1.

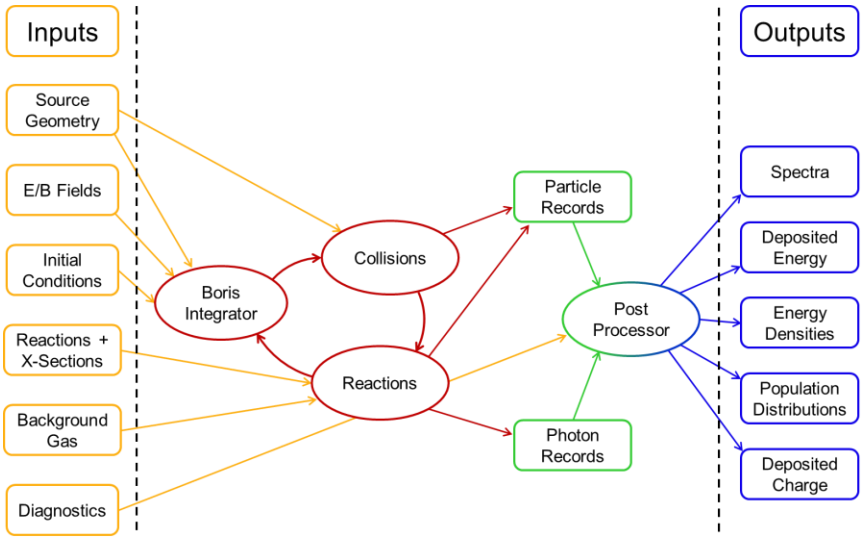

FIGURE 1. Flow diagram of BBCNI showing required inputs, computation modules, and possible output data.

To the left of Fig. 1 are the inputs required by BBCNI for a full simulation of a large ion beam. Source geometry and information on the diagnostics are obtained from details of the experiment to be simulated. The background gas density is currently calculated using an in-house gas flow simulation, and energy dependent cross sections are specified as analytic fits to the incident particle energy [16,17,18]. Magnetic fields generated by permanent magnets are calculated using the PerMag code [19], and Ansys is used to calculate those generated by DC currents. The required electric fields are calculated for each aperture using IBSimu [20] from specified grid voltages, current densities, and the same magnetic fields as BBCNI. It is ensured that IBSimu and BBCNI also use the same initial conditions as far as possible, as they are known to affect the calculated fields, including the 3 eV starting energy required by IBSimu.

As BBCNI should be able to link features seen in diagnostic results with beamlet level phenomena, there are a number of features that have been included to ensure this is done as accurately as possible. In particular, it is possible to provide a unique 3D electric field map for each aperture. It is also ensured that all records of particles, reactions, or photons, are traceable to the originating aperture and particle. This means statistical analyses can be performed on results from specific apertures, or groupings of apertures, and so a differentiation made between those effects that actually occur at the beamlet level, and those that appear simply because of the mixing of information between beamlets.

The BATMAN Upgrade Test Facility

In order to demonstrate some of the possibilities for forward diagnostic calculation with BBCNI, simulations of the BATMAN Upgrade Test Facility (BUG) were performed. This facility has recently been brought into operation at IPP Garching [9,10], and consists of the IPP Prototype Source [21] coupled to a 5×14 aperture, 4 grid extraction system, as shown in Fig. 2. This figure gives a brief overview of the test facility and the beam diagnostics available, as well as a cross section of one aperture of the grid system, including definitions of the extraction voltage (U_{ex}) and acceleration voltage (U_{acc}). For further details on the plasma source and extraction system, see [10].

The beam diagnostics relevant for this work are the beam dump calorimeter, located 2.1 m from the grounded grid (GG), and the second set of beam emission spectroscopy (BES) collection optics, which are located 1.6 m from the GG. The copper beam dump calorimeter is separated into 4×4 cm sections, some of which contain embedded thermocouples for a measurement of the profile of the beam power density. The BES collection optics are located in a vertical array, each collecting light from a horizontal line of sight subtending an angle of 57° with the beam. This angle is required to provide a sufficient Doppler shift of the collected light, so that the various peaks in the resulting spectra can be spectroscopically distinguished. The 5 lines of sight from which data will be shown are at vertical positions of −12 cm, −6 cm, 0 cm, 6 cm, and 12 cm, with respect to the centre line of the extraction system.

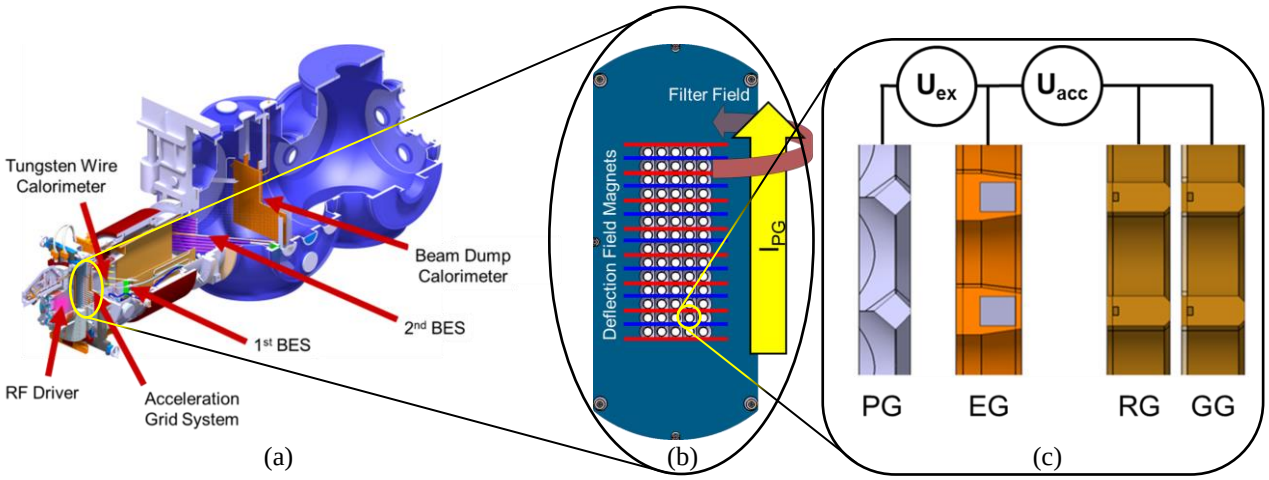

FIGURE 2. (a) Layout of the BATMAN Upgrade Test Facility including beam diagnostics; (b) view of the Plasma Grid (PG) showing aperture layout and magnetic fields present in extraction system; (c) cross section through the acceleration system grids, showing PG, Extraction Grid (EG), Repeller Grid (RG), and Grounded Grid (GG). Also shown are the electrical connections for extraction voltage (U_{ex}) and acceleration voltage (U_{acc}).

As in other large negative ion sources, a magnetic filter field is used in the plasma expansion region to cool the plasma and reduce the number of co-extracted electrons. This is generated by either permanent magnets attached to the side of the expansion region, or by flowing a current of up to 3 kA vertically through the plasma grid (PG). In either case, the field is also present in the extraction system, which causes a vertical deflection of the ions in each beamlet. Permanent magnets are embedded in the extraction grid (EG), the alternating polarity of which is shown in Fig. 2(b). These generate a vertical deflection field to remove any remaining co-extracted electrons from the beam. This field also causes a sideways deflection of the beamlets that alternates by aperture row.

Examples of Diagnostic Capabilities

The simulations of BUG performed with BBCNI were designed to recreate actual experiments at the test stand. Accordingly, the parameters used for all calculations were the same as those measured, with U_{ex} = 5.7 kV and a source pressure of 0.4 Pa. The filter field was generated either with the permanent magnets, or by 2.2 kA of current through the PG (I_{PG}). In both cases, the field strength is similar in the extraction region - about 4 mT - but the polarity on the downstream side of the plasma grid is different. U_{acc} was varied between 7.5 kV and 32.5 kV. For each set of parameters, individual 3D electric field maps were calculated for each aperture using IBSimu. Unlike in the experiment however, the extracted current density, j_{ex}, of each aperture was equal to the experimentally measured average current density, 12.8 mA·cm^{-2}. Nonuniform extraction is something that is not yet implemented into BBCNI, but will be in a future version. Thus the results from the simulations are not expected to agree exactly with the experiment, but can still provide valuable insight into the complexity of the diagnostic data and analysis thereof. The diagnostics in the simulation were the same as in the experiment, as described in the previous section. In the present section, results are given from the simulation with U_{acc} = 20 kV and the filter field generated by 2.2 kA of I_{PG}.

Diagnostic Planes

Figure 3 shows the energy density of the beam for two diagnostic planes in the simulation. The energy density on the calorimeter is given in Fig. 3(a). In the left half of the image is what would be seen by an infrared camera observing the calorimeter with its 4×4 cm blocks. The right section of the image is binned at 1×1 cm, showing greater detail and allowing the more accurate estimation of the size of the beam and the position of the beam centre. The downward shift from the filter field can be clearly seen, as can the tall and narrow shape of the beam due to the arrangement of apertures in the extraction system.

The calorimeter could in principle be shown with any size bins, or limited to showing only energy from incident H atoms, or only from a certain collection of apertures. As the diagnostic calorimeter in the simulation is simply a

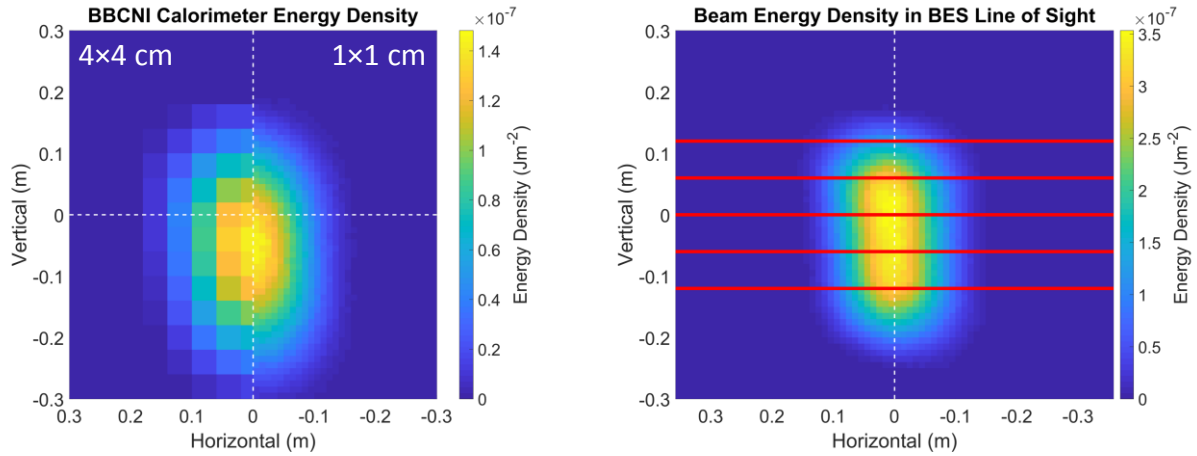

FIGURE 3. Energy density of the beam (a) striking the beam dump calorimeter and (b) passing through the plane containing the BES lines of sight.

detection of when particles pass a certain point, it is a trivial matter to move this point, or to have the detection area at an angle to the beam. This is demonstrated in Fig. 3(b), which shows the beam energy density passing through the vertical plane containing the BES lines of sight. This plane is therefore tilted at an angle of 57° with respect to the beam, with the left hand side of the image being closer to the GG than the right. As the beam is deflected downward due to the filter field, this causes it to appear asymmetric in Fig. 3(b). While most of the BES lines of sight pass through the most intense region of the beam, the vertical deflection causes the top line of sight to miss the bulk of the beam. This affects not only the amount of recorded light, but also the population of particles sampled by it.

Spectroscopy of Large Beams

Examples of the simulated spectra that can be obtained and results that can be calculated from the collection of spectra in the simulation are given in Fig. 4. Labelled in Fig. 4(a) are the features expected from such a spectrum. The Doppler peak stems from the collisional excitation of full-energy H atoms (either directly or via collisional detachment of H^-) and their subsequent H_α emission. The stripping peak is from H atoms created during the acceleration of the ions in the beamlet, when the parent H^- is not yet fully accelerated, and so has less than the

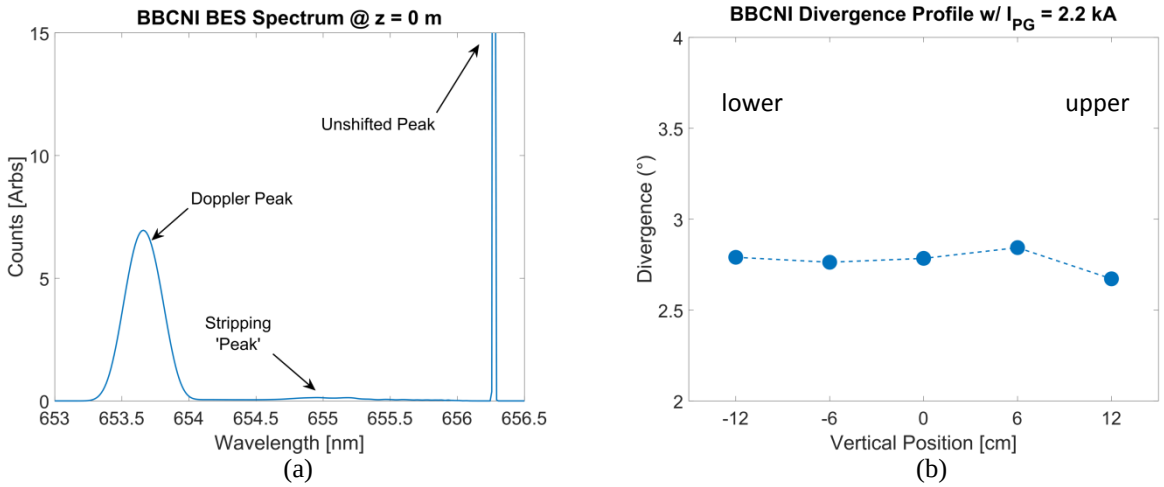

FIGURE 4. Examples of (a) a BES spectrum as recorded from the central line of sight and (b) the vertical profile of beam divergence as calculated from simulated spectra.

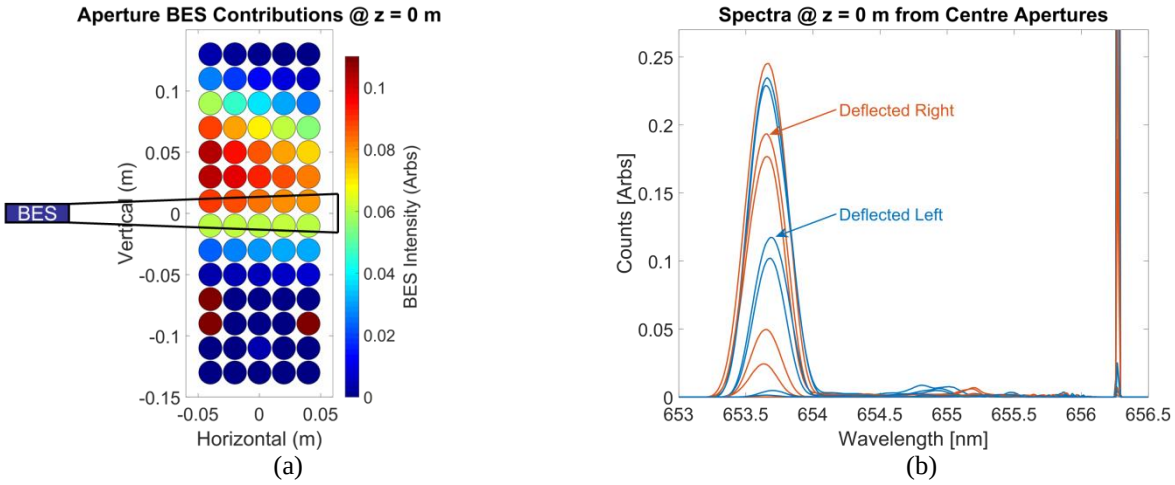

FIGURE 5. Detailed analysis of the spectrum measured by the central line of sight showing (a) the relative intensity contributions from each aperture to the total spectrum, and (b) actual spectra generated by individual apertures, grouped by polarity of the deflection field. This shows how both the horizontal and vertical position of the aperture affects the spectra.

maximum energy of the beam. From this stripping peak it is possible to obtain an estimate of the fraction of H^- that are neutralised, or 'stripped', inside the extraction and acceleration system. This can not only degrade the intensity of the beam, but is also important for the quality of the beam. It is also important to avoid excessive heat loading on the grid system due to the impact of the resulting electrons. The unshifted peak is from collisionally excited slow particles of the background gas, but currently has no broadening mechanisms in BBCNI.

The Doppler shift of an incident photon is a function of the energy of the emitting particle and the velocity of the particle relative to the collection optics. In the case of the Doppler peak labelled in Fig. 4(a), it is usually assumed for the experimental analysis that the particles are mono-energetic, and so the width of the peak can be used to estimate the divergence of the beam. This evaluation of the divergence from the Doppler peak width can be performed on the synthetic spectra calculated by BBCNI to provide a direct comparison point with experimental data. This was performed for the 5 vertically arranged lines of sight, the results of which are shown in Fig. 4(b). In this profile it can be seen that the measured divergence is not uniform, with the uppermost point measuring a slightly lower divergence than the other lines of sight. However this is to be expected, as, as shown in Fig. 3(b), this line of sight is scraping the very top of the beam. As the beam is expected to be uniform otherwise, a simple expectation would be for the measured divergence from the other lines of sight to also be uniform. However, with only the information available in Fig. 4, it is not possible to discern whether the observed slight variation is a real effect, or an artefact of the diagnostic.

Figure 5 shows an analysis of how different apertures contribute to the spectrum measured by the simulated line of sight observing the vertical centre of the extraction area. There are two obvious differences between the map of aperture intensity in Fig. 5(a) and the naïve expectation of what it should look like. Firstly, although the data is for the line of sight in the vertical centre, the most light is collected from apertures above the centre line. This is a result of the downward beam deflection due to the filter field. The second clear difference is the trend for higher intensity from apertures to the left of the image. As the horizontal distance from the collection optics to the centre of the beam is 38.5 cm, the 8 cm variation between the left- and right-most apertures is a significant fraction of this. Thus the beamlets from apertures closer to the collection optics, in this case on the left of the image, subtend a noticeably larger solid angle with the entrance to the optics, and so deliver more light to the measurement.

Some of the consequences on the spectra can be seen in Fig. 5(b), which shows the spectra from the central column of apertures, as collected by the line of sight in the vertical centre. Not only do the spectra have different intensities, as seen in Fig. 5(a), but the widths and central wavelengths of the Doppler peaks also differ by small but noticeable amounts. The change in central wavelength of the peak is caused mostly by the alternating deflection field. This has been highlighted by colouring the spectra according to the direction in which the beamlet is deflected. The different heights and small changes in peak widths are due to different population sampling of the beamlets, which is seen on a whole-beam level in Fig. 4(b).

It is also important to realise that even these individual peaks are not necessarily Gaussian, although they appear so in this case. There are a variety of effects that can cause the velocity distribution of the individual beamlets to differ from a Gaussian. As a result of this, the total Doppler peak that is observed in experiment or seen in the simulation is unpredictably non-Gaussian. As a Gaussian fitting is used to analyse the diagnostic data, this could

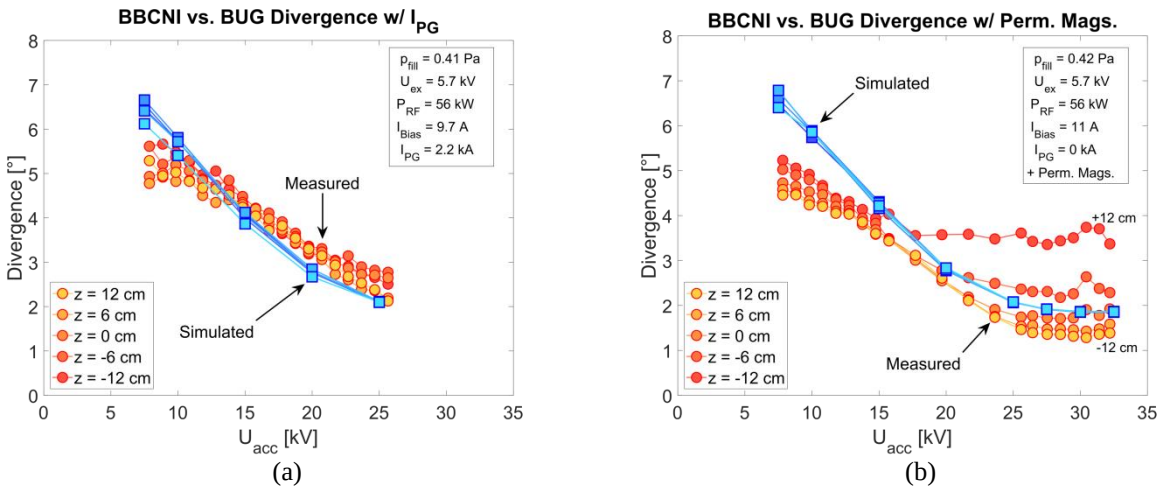

FIGURE 6. Comparison of simulated (BBCNI - □) and experimental (BUG - ○) measurements of divergence from BES data vs U_{acc}. Two different magnetic filter fields are used: (a) I_{PG} and (b) permanent magnets.

result in an overestimation of the measured divergence.

COMPARISON WITH PRELIMINARY BUG RESULTS

As part of the commissioning and conditioning process for BATMAN Upgrade, two scans in U_{acc} were performed, while holding other parameters as constant as possible. The two scans were performed with the same two different configurations of magnetic filter field described previously; one with 2.2 kA of I_{PG}, and one with permanent magnets attached to the outside of the expansion region.

With U_{ex} held at 5.7 kV, U_{acc} was increased until breakdowns began occurring in the grid system. As was mentioned, and is important to stress, these experiments were performed as part of the commissioning process of the system, and such breakdowns are a normal part of the commissioning process.

Figure 6 shows the divergences calculated from both simulated and experimental spectra as a function of U_{acc} for the 5 BES lines of sight, and for both configurations of the filter field. The general trend is for a decreasing measured divergence across the whole beam with increasing U_{acc}. As expected, this trend levels off at the higher values of U_{acc} for both the experimental and simulation cases with permanent magnets, shown in Fig. 6(b). This suggests an optimum ratio between U_{acc} and U_{ex} of around 5.5.

However, there are also differences between the two experimental scans. In particular, while Fig. 6(a) shows a roughly uniform divergence profile, the scan performed with permanent magnets is clearly far from uniformity. Langmuir probe measurements have shown that plasma nonuniformity is stronger in the case of permanent magnets that while using I_{PG} [22]. This indicates, as discussed in the introduction, that the plasma uniformity plays a role in the homogeneity of the extracted current, and so the beam divergence. The inhomogeneity of the divergence when permanent magnets are installed is greatest for the higher values of U_{acc}, although the reasons for this are not yet known. As nonuniformities in extracted current are not included in BBCNI, the individual lines of sight in the simulation give very similar results. This holds across simulation results for both scans.

For low U_{acc}, below around 15 kV, some nonuniformity is observed in the measured divergence for both simulated and experimental data. At these low voltages, the Doppler peak becomes increasingly non-Gaussian. As a result, so the calculated divergence becomes increasingly susceptible to changes to the peak shape, and therefore to any experimental or statistical noise that may be present. In addition, the intensity of the measured light decreases significantly, so that the signal to noise ratio in the experiment starts to affect the results. This can be seen especially in the left side of Fig. 6(a), where the experimental results become somewhat erratic.

Despite the unrealistic assumption of homogeneous j_{ex} in BBCNI, the agreement between the simulated and experimental results is good. Where the spread is large in the experimental data, the simulation results lie closest to those from the central line of sight in the experiment. This shows that with homogeneous extraction, BBCNI is able to recreate well the behaviour of the beamlets with close to the average value of j_{ex}, and accurately simulate the diagnostics of a collection of beamlets.

CONCLUSIONS

It has been shown that through the use of a 3D particle tracking code, BBCNI, a forward calculation of synthetic diagnostic data can be performed from particle level information on large negative ion sources. The results from these simulated diagnostics are seen to conform to experimental data for a wide range of source parameters, despite the effects of plasma nonuniformity being omitted from the simulation.

The simulated diagnostic results are built from particle level data with a full 3D consideration of each aperture in the source and the beamlet it generates. With a full traceability of diagnostic information to the originating aperture and particle, it can be determined with such a code which of the phenomena observed in diagnostic data are real, and which are artefacts from the mixing of beamlets with different properties. For example, it has been shown in this work how the unique beam emission spectra of individual apertures can combine into a potentially non-Gaussian Doppler peak, from which overestimated divergences values could be calculated.

By supplementing experimental results with an understanding of the reasons behind those results, research efforts can be directed toward the most likely candidates for improving beam quality. This will become ever more important as negative ion sources increase in size and have a greater number of apertures. While BBCNI is currently configured to assist with the understanding of beam diagnostics on the BATMAN Upgrade test facility at IPP, it is designed to be flexible, and could in principle be applied to any large ion source, and will be applied to ELISE in the near future. With the foreseen inclusion of inhomogeneous extracted current density, BBCNI will provide a powerful tool for the further improvement of these large ion sources.

REFERENCES

1. R. Hemsworth *et al*, *New J. Phys.* **19**, 025005 (2017).
2. B. Heinemann *et al*, Fusion Eng. Des. (2018), DOI: 10.1016/j.fusengdes.2018.03.025 (In Press)
3. V. Toigo *et al*, *New J. Phys.* **19**, 085004 (2017).
4. U. Fantz et al, *Nucl. Fusion* **57**, 116007 (2017)
5. U. Fantz, L. Schiesko, and D. Wünderlich, *Plasma Sources Sci. Technol.* **23**, 044002 (2014)
6. A. Mimo, C. Wimmer, D. Wünderlich, and U. Fantz, *AIP Conf. Proc.* **1869**, 030019 (2017)
7. P. Franzen and U. Fantz, *AIP Conf. Proc.* **1390**, 310-321 (2011)
8. B. Zaniol, R. Pasqualotto, and M. Barbisan, *Rev. Sci. Instrum.* **83**, 043117 (2012)
9. B. Heinemann et al, *AIP Conf. Proc.* **1655**, 060003 (2015)
10. W. Kraus, U. Fantz, B. Heinemann, L. Schiesko, C. Wimmer, and the NNBI Team, this conference.
11. F. Taccogna, P. Minelli, and S. Longo, *Plasma Sources Sci. Technol.* **22**, 045019 (2013)
12. R. Nocentini, R. Gutser, B. Heinemann, M. Froeschle, and R. Riedl, *Fusion Eng. Des.* **84**, 2131-2135 (2009)
13. Y. Takeiri et al, *Rev. Sci. Instrum.* **66**, 5236-5243 (1995).
14. P. Agostinetti et al, *Nucl. Fusion* **56**, 016015 (2015)
15. B. Ruf, P. Franzen and U. Fantz, *40th EPS Conference on Plasma Physics* (2013).
16. C. F. Barnett *et al*, *NASA STI/Recon Technical Report N* **91** (1990).
17. J. Geddes, J. Hill, and H. B. Gilbody, *J. Phys. B: At. Mol. Phys.* **14**, 4837 (1981).
18. T. Tabata and T. Shirai, *At. Data Nucl. Data Tables* **76**, 1–25 (2000).
19. D. Ciric, private communication, UKAEA Fusion/Euratom Association, Abingdon, UK, 2007.
20. T. Kalvas *et al*, *Rev. Sci. Instrum.* **81**, 02B703 (2010).
21. W. Kraus et al, *Rev. Sci. Instrum.* **83**, 02B104 (2012).
22. L. Schiesko, C. Wimmer, U. Fantz, and the NNBI Team, this conference.